

# Multistate Photochemical Reaction Dynamics of ClNO in Solution: An Absolute Resonance Raman Intensity Analysis Study<sup>†</sup>

Bethany P. Nyholm and Philip J. Reid\*

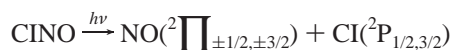
Department of Chemistry, Box 351700, University of Washington, Seattle, Washington 98195

Received: November 26, 2003; In Final Form: January 30, 2004

The excited-state reaction dynamics of nitrosyl chloride (ClNO) are studied using absolute resonance Raman intensity analysis. The absolute resonance Raman cross sections for ClNO dissolved in cyclohexane and acetonitrile are measured at several excitation wavelengths spanning the absorption band commonly referred to as the “A band” ( $\lambda_{\text{max}} \approx 200$  nm). The resonance Raman and absorption cross sections are modeled using the time-dependent formalism. Resonance Raman depolarization ratios are also measured and are found to be consistent with at least two electronic transitions participating in the scattering process. Therefore, the standard time-dependent formalism approach was modified by incorporating two excited states into the analysis, with state contributions deconvolved through modeling of the depolarization ratios in addition to the absolute resonance Raman and absorption cross sections. The spectroscopic observables are well reproduced using this two-state model. The analysis presented here demonstrates that the photoexcitation of solution-phase ClNO results in a substantial evolution of the N–Cl stretch coordinate consistent with the dissociation of the N–Cl bond. Significant structural evolution is also observed along the bend, with minimal excited-state structural evolution observed along the N=O stretch. The structural evolution along the dissociative N–Cl stretch coordinate is found to be solvent-dependent, and the origin of this dependence is related to changes in the ground-state equilibrium geometry as a function of solvent environment. Finally, the homogeneous line width undergoes a significant increase in acetonitrile relative to cyclohexane, and this increase is proposed to reflect the modification of the excited-state interactions and nonadiabatic relaxation dynamics.

## Introduction

The photochemistry of nitrosyl halides such as nitrosyl chloride (ClNO) is of interest because of the participation of these compounds in stratospheric and tropospheric chemistry.<sup>1,2</sup> ClNO is formed in the lower atmosphere by the reaction of sea salt (NaCl) with NO<sub>2</sub> and in the upper troposphere/stratosphere via surface reactions of HONO on frozen HCl.<sup>3</sup> The gas-phase photochemistry of ClNO is dominated by dissociation to form NO and Cl with a quantum yield approaching unity.<sup>1,4–15</sup>



The vis–UV absorption spectrum of ClNO is characterized by a series of absorption bands extending from  $\sim 650$  nm into the UV. These transitions are referred to as the K through A bands as one proceeds from low to high energy.<sup>16,17</sup> Studies of gaseous ClNO have provided a detailed understanding of the dissociation dynamics that occur following photoexcitation resonant with all transitions except the highest-energy A band.<sup>18,19</sup> Although the A-band transition ( $\lambda \approx 180$  to 250 nm) is by far the most intense ( $\sigma_{\text{A,max}} = 6.5 \times 10^{-17}$  cm<sup>2</sup>), it is the least studied.<sup>17</sup> The substantial absorption cross section and breadth that characterize the A band suggest that more than a single electronic transition contributes to the observed intensity.<sup>12,14,15</sup> Consistent with this suggestion, photodissociation studies have observed an evolution in photofragment anisotropy with increased actinic energy

through the A band consistent with multiple states participating in the dissociation process.<sup>12,14</sup> An evolution in photoproduct anisotropy can occur for dissociation reactions mediated by a single excited state if a substantial amount of rotational energy is deposited into the diatomic photofragment; however, studies of the Cl-product velocity distribution demonstrated that the anisotropy is independent of the kinetic energy released into the products, consistent with the multiple-state model.<sup>15,20–22</sup> Also supporting the multistate model, *ab initio* studies have predicted that multiple transitions exist in this wavelength region associated with the A band.<sup>8,23,24</sup> In contrast, resonance Raman studies of gaseous ClNO have been interpreted in terms of the A band being composed of a single excited state.<sup>25</sup>

Only a handful of ClNO photochemical studies in condensed environments have been performed. Matrix isolation studies have demonstrated ClON production following ClNO photoexcitation.<sup>26,27</sup> Surface-photochemical studies of ClNO have observed N–Cl bond dissociation leading to the formation of NO and Cl.<sup>28</sup> Comparative matrix and gas-phase Raman studies of ClNO have documented frequency shifts of the Raman transitions between these two environments demonstrating that the curvature of the ground-state potential energy surface is environment-dependent.<sup>29–31</sup> In a previous study, we reported the resonance Raman depolarization ratios for ClNO dissolved in cyclohexane employing excitation resonant with the A band.<sup>32</sup> The experimentally determined depolarization ratios were not equal to  $1/3$ , consistent with more than a single excited state contributing to the observed scattering; however, the nature of these states including the extent of electron–photon coupling and the solvent dependence of the state curvature and energetics was not explored.

<sup>†</sup> Part of the special issue “Alvin L. Kwiram Festschrift”.

\* To whom correspondence should be addressed. E-mail: preid@chem.washington.edu. Fax: (206) 685-8665.

In this paper, we present an absolute resonance Raman intensity analysis study of ClNO dissolved in cyclohexane and acetonitrile. In this study, resonance Raman depolarization ratios, absorption, and Raman cross sections are measured at excitation wavelengths spanning the A band. Similar to our previous studies, the depolarization ratios are observed to deviate significantly from  $1/3$  in both solvents, consistent with more than a single electronic transition contributing to the A band.<sup>32</sup> Therefore, modeling of the experimental observables was performed by employing two excited states, with the inclusion of depolarization ratios in the modeling process providing a methodology by which to separate the state contributions. Studies were performed in cyclohexane and acetonitrile because we are particularly interested in the effect of solvent polarity on the excited-state reaction dynamics of this system. The analysis of the ClNO absorption and resonance Raman cross sections in both solvents demonstrates that the A-band transition undergoes a significant decrease in frequency and broadens in acetonitrile relative to its behavior in cyclohexane. The two-state model outlined here is capable of reproducing this behavior and suggests that this evolution is due to differential excited-state solvation. The modeling also shows that the excited-state structural evolution that occurs in both excited states following photoexcitation is dominated by evolution along the dissociative N–Cl stretch and bend coordinates in both solvents. Minimal resonance Raman intensity is observed corresponding to the N=O stretch, consistent with limited excited-state structural evolution along this coordinate. A comparison of the model excited-state parameters in cyclohexane and acetonitrile reveals that the excited-state slope of the N–Cl stretch coordinate decreases in acetonitrile relative to cyclohexane. As will be discussed below, the solvent dependence of the excited-state slope results in a modification of the ground-state N–Cl bond length as a function of the environment. Finally, the resonance Raman cross sections are significantly lower in acetonitrile than in cyclohexane, consistent with increased homogeneous broadening in acetonitrile. In total, the results presented here provide the first information regarding the early-time, A-band photochemical reaction dynamics of ClNO in solution.

## Experimental Section

**Materials.** The absolute resonance Raman intensities of nitrosyl chloride (ClNO) dissolved in acetonitrile (Fisher, 99.9+%) and cyclohexane (Aldrich, 99.9+%) were measured at 192.2, 204.3, 208.9, 217.8, 228.7, 252.7, 282.4, and 354.7 nm using the direct or hydrogen-shifted second and third harmonic output of a Nd:YAG laser (Spectra-Physics GCL-170, 30 Hz). The location of these wavelengths relative to the A band are indicated in Figure 1. The synthesis of gaseous ClNO has been described elsewhere.<sup>32,33</sup> Briefly, 8.75 g of sodium nitrite (99.9% reagent grade, Aldrich) was dissolved in 12.5 mL of water and added dropwise to 50 mL of concentrated hydrochloric acid (Fisher). The solution was stirred continuously, and the production of ClNO was evidenced by the appearance of an orange-brown gas. Gaseous ClNO was bubbled through solvent to produce the samples for study. Static vis–UV absorption was used to determine sample purity. The ClNO concentration was adjusted to between 0.1 and 4 mM depending on the excitation wavelength employed.

**Resonance Raman Spectra.** Resonance Raman spectra of ClNO in cyclohexane and acetonitrile were obtained by employing a quartz flow cell equipped with sapphire entrance and exit windows. The sample flow rate was sufficient to replace the

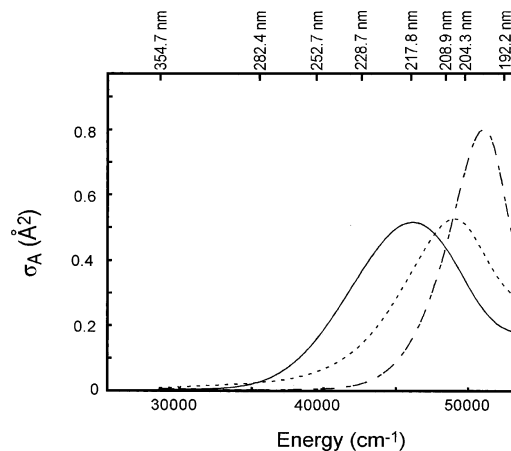


**Figure 1.** Absorption spectra of gaseous ClNO (—), ClNO dissolved in cyclohexane (---), and ClNO dissolved in acetonitrile (— · —). The gaseous ClNO spectrum is in excellent agreement with the literature.<sup>17</sup> Also indicated are the excitation wavelengths employed in the resonance Raman studies.

illuminated volume between excitation pulses. The scattered light was collected using refractive UV-quality optics and delivered to a 0.75-m spectrograph (Acton). The scattered light was dispersed using either a 1200-groove/mm classically ruled, a 2400-groove/mm holographic, or a 3600-groove/mm holographic grating. A polarization scrambler was placed at the spectrograph entrance to minimize the polarization dependence of the spectrometer throughput. Detection was performed using a 1100 pixel  $\times$  300 pixel, back-thinned, liquid-nitrogen-cooled CCD detector (Princeton Instruments). The concentration of the sample was measured before and after each experiment to ensure that sample photodegradation was  $<10\%$ .

**Depolarization Ratios.** The resonance Raman depolarization ratios for the bend and N–Cl stretch fundamental transitions in acetonitrile and cyclohexane were measured at 217.8, 228.7, 252.7, 282.4, and 354.7 nm. The depolarization ratio is defined as the intensity of scattered light with polarization perpendicular to that of the incident radiation divided by the intensity of light scattered with polarization parallel to that of the excitation light.<sup>34</sup> The incident polarization was defined by placing an  $\alpha$ -BBO polarizer in the path of the excitation beam. Nonbirefringent CaF<sub>2</sub> windows were placed on the quartz sample cell to preserve the polarization of the incident and scattered fields. A large-aperture, 1.5-cm-diameter Glan-Taylor calcite polarizer was placed before the polarization scrambler to define the polarization of the scattered light delivered to the spectrograph. The depolarization ratio of the 802-cm<sup>-1</sup> transition in cyclohexane or the 918-cm<sup>-1</sup> transition of acetonitrile was measured at each wavelength to correct for the nonideal extinction of the polarizer as described previously.<sup>35</sup>

**Intensity Corrections.** A standardized deuterium lamp (Hellma) was used to correct the scattered intensities for the wavelength sensitivity of the detection apparatus. Correction for scattering self-absorption was performed by comparing the solvent peak intensities between spectra of neat solvent and spectra with ClNO present. This correction resulted in a minimal ( $<2\%$ ) change in the measured intensities.

**Absolute Raman Cross-Section Determination.** ClNO absolute resonance Raman cross sections were determined by comparison to the 802-cm<sup>-1</sup> transition of cyclohexane or the 918-cm<sup>-1</sup> transition of acetonitrile. The later transition was standardized by comparison to the CN stretch transitions of acetonitrile (2150–2350 cm<sup>-1</sup>) for which the absolute scattering

cross sections have been previously reported.<sup>36,37</sup> The details of this standardization are presented below. The absolute resonance Raman scattering cross sections of CINO were determined by comparison to the solvent using the following equation:

$$\sigma_{\text{CINO}} = \frac{I_{\text{CINO}} C_{\text{solvent}} \left( \frac{1+2\rho}{1+\rho} \right)_{\text{CINO}}}{I_{\text{solvent}} C_{\text{CINO}} \left( \frac{1+2\rho}{1+\rho} \right)_{\text{solvent}}} \sigma_{\text{solvent}} \quad (1)$$

In eq 1,  $\sigma$  is the Raman scattering cross section,  $\rho$  is the depolarization ratio,  $c$  is the concentration, and  $I$  is the scattered intensity. Depolarization ratios for the solvent were taken from the literature:  $\rho = 0.08 \pm 0.01$  for the 802-cm<sup>-1</sup> transition of cyclohexane,  $\rho = 0.025 \pm 0.003$  for the 918-cm<sup>-1</sup> transition of acetonitrile, and  $\rho = 0.036 \pm 0.005$  for the CN stretches (2150–2350 cm<sup>-1</sup>) of acetonitrile.<sup>36–38</sup> Depolarization ratios for CINO were obtained as described above. Scattered intensities were determined by trapezoidal integration to determine peak areas. The absolute scattering cross section of the CINO bend fundamental transition was determined at all wavelengths by comparison to solvent, and the cross sections for other CINO transitions were determined by comparison to the bend fundamental.

**Computational Analysis.** The absorption and resonance Raman cross sections were modeled using the time-dependent formalism for absorption and resonance Raman scattering.<sup>39–41</sup> A modified version of the time-dependent formalism was employed here, in which two excited states are included in the modeling:<sup>42</sup>

$$\sigma_{\text{R}}(E_1) = \frac{8\pi e^4 E_s^3 E_1}{9\hbar^6 c^4} \left| \int_0^\infty M_1^2 \langle f|i_1(t) \rangle e^{i(E_1+E_s)t/\hbar} D_1(t) dt + \int_0^\infty M_2^2 \langle f|i_2(t) \rangle e^{i(E_1+E_s)t/\hbar} D_2(t) dt \right|^2 \quad (2)$$

$$\sigma_{\text{A}}(E_1) = \frac{4\pi e^2 E_1}{6\hbar^2 cn} \left[ \int_{-\infty}^\infty M_1^2 \langle i|i_1(t) \rangle e^{i(E_1+E_s)t/\hbar} D_1(t) dt + \int_{-\infty}^\infty M_2^2 \langle i|i_2(t) \rangle e^{i(E_1+E_s)t/\hbar} D_2(t) dt \right] \quad (3)$$

In eqs 2 and 3,  $E_s$  and  $E_1$  are the scattered and incident frequencies, respectively, the transition moments for the two electronic transition lengths are given by  $M_1$  and  $M_2$ ,  $c$  is the speed of light,  $n$  is the refractive index,  $E_f$  is the energy of the final state,  $f$ , and  $E_i$  is the energy of the initial state,  $i$ . The initial state propagating for time  $t$  on the  $n$ th excited-state surface is indicated by  $|i_n(t)\rangle = e^{-iH_n t/\hbar} |i\rangle$ . Homogeneous broadening corresponding to each excited state is given by  $D_1(t)$  and  $D_2(t)$  and is modeled as Gaussian ( $e^{-\Gamma^2 t^2/\hbar^2}$ , where  $\Gamma$  is the homogeneous line width). Equation 3 demonstrates that the resonance Raman cross section is dependent on the sum of the polarizability derived from the two excited states. The polarizability is in turn dependent on the half Fourier transform of the overlap,  $\langle f|i(t)\rangle$ , representing the overlap of the final state involved in the scattering process with the initial state propagating under the influence of the excited-state Hamiltonian. These expressions demonstrate that both the Raman and absorption cross sections depend on time-dependent overlap terms involving two excited states. The time-dependent overlaps were determined by employing harmonic surfaces for the bend and the NO stretch and a linearly dissociative surface for the N–Cl stretch. Time-

dependent overlaps along the bend and NO stretch were calculated using the formalism of Mukamel and co-workers.<sup>43</sup> Time-dependent overlaps along the N–Cl stretch were calculated as described in the literature.<sup>40,44</sup> In calculating the Raman cross section, the contributions from each excited state are added at the amplitude level such that interference can occur, leading to the reduction or enhancement of the scattering cross sections depending on the sign of the displacements. Both excited states are modeled as dissociative along the N–Cl coordinate. The displacements along the bend and NO stretch coordinates were taken to be similar in sign between the two states as well. This assumption was checked by testing a model that included displacements of opposite sign for the two states along the various transitions, and a reasonable fit could not be obtained.

Resonance Raman depolarization dispersion curves were modeled as follows. In the limit of two excited states participating in the scattering process having orthogonal transition moments, the depolarization ratio ( $\rho$ ) is defined as<sup>32,45</sup>

$$\rho = \frac{I_{\text{per}}}{I_{\text{par}}} = \frac{3 \sum^2}{10 \sum^0 + 4 \sum^2} \quad (4)$$

In eq 4, the  $\sum^n$  terms are given by

$$\sum^0 = \frac{1}{3} |\alpha_{xx} + \alpha_{yy}|^2 \quad (5)$$

$$\sum^2 = \frac{1}{3} \{ |\alpha_{xx} - \alpha_{yy}|^2 + |\alpha_{xx}|^2 + |\alpha_{yy}|^2 \}$$

where  $\alpha_{pp}$  ( $p = x, y$ ) are the elements of the polarizability tensor. Equations 4 and 5 correspond to the following conceptual picture. If coupling between the two excited states is negligible, then the two transitions will give rise to two diagonal elements of the polarizability tensor ( $\alpha_{xx}$  and  $\alpha_{yy}$ ). Each polarizability tensor is described using the time-dependent formalism as follows:<sup>39–41</sup>

$$[\alpha_{\text{it}}(E_L)]_{pp} = \frac{ie^2 M_{pp}^2}{\hbar} \int_0^\infty \langle f|i(t) \rangle e^{i(E_L+\epsilon_i)t/\hbar} D(t) dt \quad (6)$$

In eq 6,  $E_L$  is defined as the incident frequency,  $M_{pp}$  is the electronic transition length ( $p = x$  or  $y$ ), and the energy of the vibrational state is given by  $\epsilon_i$ .  $D(t)$  is the homogeneous line width, and  $\langle f|i(t)\rangle$ , the final state involved in the scattering process with the initial vibrational state propagating under the influence of the excited-state Hamiltonian.

If A-band intensity is derived from a single excited state, then only one of the tensor elements is finite, and  $\rho = 1/3$ . However, when a second orthogonal transition contributes,  $\rho$  will deviate from  $1/3$ . It should be noted that the deviation of  $\rho$  from  $1/3$  also could reflect preresonance contributions to the scattered intensity from electronic states located in the far-UV. Attempts to reproduce the observed depolarization ratios using preresonance effects resulted in predicted transition moments or  $E_{00}$  energies for the far-UV state that were entirely inconsistent with the absorption spectra of gaseous CINO.<sup>46</sup>

## Results

**Absorption Spectra.** The absorption spectra of gaseous CINO and CINO dissolved in cyclohexane and in acetonitrile are presented in Figure 1. The intense transition evident in the figure is the A band. This transition broadens and undergoes a 22-nm red shift in going from the gas phase to acetonitrile, with

**TABLE 1: Absolute Raman Cross Sections for the 918-cm<sup>-1</sup> Transition of Acetonitrile<sup>a</sup>**

excitation wavelength (nm)	cross section ( $\mu\text{b}$ ) <sup>b</sup>
192.2	980 $\pm$ 60
204.3	655 $\pm$ 5
208.9	550 $\pm$ 50
217.8	440 $\pm$ 50
228.7	380 $\pm$ 30
252.7	220 $\pm$ 20
282.4	95 $\pm$ 10
354.7	34 $\pm$ 2

<sup>a</sup> Absolute Raman scattering cross sections were determined by comparison to the CN stretches of acetonitrile (2150–2350 cm<sup>-1</sup>) as described in the text. <sup>b</sup> Errors represent 1 standard deviation from the mean.

cyclohexane demonstrating intermediate behavior. However, the integrated intensity of the A band remains constant, consistent with the increased breadth not arising from the presence of a new electronic transition. The measured absorption maximum of gaseous ClNO is in agreement with the literature value of  $\lambda_{\text{max}} = 196$  nm.<sup>17</sup> In cyclohexane, the A-band maximum absorption cross section is 0.53 Å<sup>2</sup> ( $\lambda_{\text{max}} = 206$  nm), and in acetonitrile the maximum cross section is also 0.53 Å<sup>2</sup> ( $\lambda_{\text{max}} = 218$  nm).

**Absolute Raman Cross Sections.** Measurement of the absolute scattering cross sections of ClNO in solution requires that the absolute scattering cross section of at least one solvent transition be known. The standardized 802-cm<sup>-1</sup> transition of cyclohexane was employed for experiments in this solvent. In acetonitrile, the 918-cm<sup>-1</sup> transition provides a convenient standard given the proximity of this transition to the ClNO transitions of interest; however, the absolute scattering cross section for this transition was unknown at all of the excitation wavelengths employed in this study. Therefore, this transition was standardized by comparison of the scattering intensity to the intensity of the CN stretch transitions for which the absolute Raman cross section are known.<sup>37</sup> The intensities and depolarization ratios of both the CN stretch (2150–2350 cm<sup>-1</sup>) and the 918-cm<sup>-1</sup> transitions of acetonitrile were measured, and the 918-cm<sup>-1</sup> transition cross section was determined using the corresponding version of eq 1 (see above). The measured scattering cross sections for the 918-cm<sup>-1</sup> transition are reported in Table 1 and are shown in Figure 2. The evolution in scattered intensity as a function of excitation wavelength for the 918-cm<sup>-1</sup> transition was fit to the following A-term expression:

$$\sigma_{\text{R}}(\nu_0) = K\nu_0(\nu_0 - \nu)^3 \left( \frac{\nu_c^2 + \nu_0^2}{(\nu_c^2 - \nu_0^2)^2} \right)^2 \quad (7)$$

In the above expression,  $\nu_0$  is the incident frequency,  $K$  is the coupling strength,  $\nu$  is the frequency of the mode of interest, and  $\nu_c$  is the energy of the excited state from which preresonant intensity is derived. The best fit resulted in  $K = 14\,712 \mu\text{b}$  (1  $\mu\text{b} = 10^{-24}$  cm<sup>2</sup>) and  $\nu_c = 130\,800$  cm<sup>-1</sup>. The far-UV absorption spectrum of acetonitrile reveals that from 70 000–90 000 cm<sup>-1</sup> there exist strong absorption bands corresponding to Rydberg transitions. However, there is little absorption present at  $\sim 130\,000$  cm<sup>-1</sup>, the fitting parameter determined by our A-term fit, but this may be due to a perturbation of Rydberg states or other electronic states now present at this energy because of solvation.<sup>37</sup>

**Resonance Raman Intensity Analysis.** Resonance Raman spectra for ClNO dissolved in cyclohexane and acetonitrile

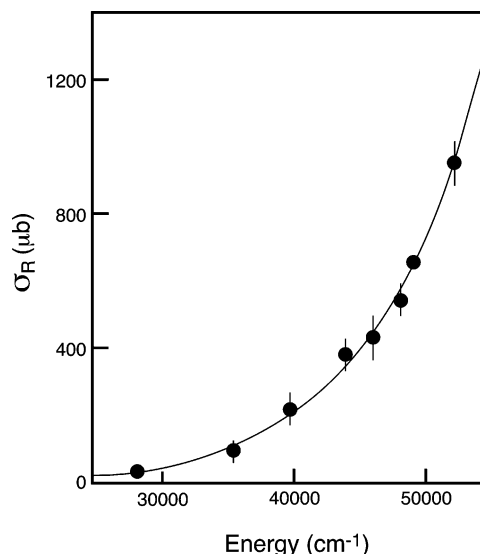


**Figure 2.** Experimental absolute Raman cross sections for the 918-cm<sup>-1</sup> transition of acetonitrile (●). Values are also presented in Table 1. Error bars represent 1 standard deviation from the mean of the total number of measurements. The A-term fit to these cross sections (eq 1 in the text) is shown by solid line.

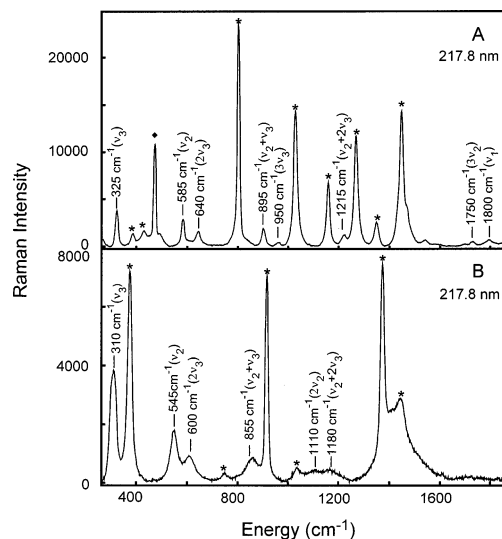


**Figure 3.** Resonance Raman spectra of ClNO dissolved in cyclohexane (A) and in acetonitrile (B) obtained using 217.8-nm excitation. Solvent transitions are marked with asterisks, and hydrogen lines from the excitation source are denoted with diamonds. Note that for cyclohexane, transitions corresponding to all three vibrational modes are observed.

obtained using 217.8-nm excitation are presented in Figure 3. Intensity corresponding to fundamental transitions of the bend ( $\nu_3$ ) and N–Cl stretch ( $\nu_2$ ) is evident in both solvents. In cyclohexane, the fundamental transition of the N=O stretch ( $\nu_1$ ) is also observed. The absolute resonance Raman cross sections measured in both solvents for these and other prominent transitions are provided in Tables 2 and 3. A comparison of the spectra presented in Figure 3 demonstrates that many more transitions are observed in cyclohexane relative to acetonitrile. As will be discussed below, this behavior is primarily due to a significant increase in the homogeneous line width in acetonitrile, resulting in the depression of the resonance Raman cross sections in this solvent. A comparison of the resonance Raman spectra obtained in two solvents also reveals that the transition frequencies are solvent-dependent. For example, the bend fundamental transition ( $\nu_3$ ) is observed in cyclohexane at  $325 \pm 3$  cm<sup>-1</sup>, but is at  $310 \pm 5$  cm<sup>-1</sup> in acetonitrile. This

**TABLE 2: Absolute Raman Cross Sections of Nitrosyl Chloride Dissolved in Cyclohexane**

excitation $\lambda$ (nm)	$\nu_1^a$ $\times 10^7(\text{\AA}^2)$	$\nu_2$ $\times 10^7(\text{\AA}^2)$	$3\nu_2$ $\times 10^7(\text{\AA}^2)$	$\nu_3$ $\times 10^7(\text{\AA}^2)$	$2\nu_3$ $\times 10^7(\text{\AA}^2)$	$\nu_2 + \nu_3$ $\times 10^7(\text{\AA}^2)$	$\nu_2 + 2\nu_3$ $\times 10^7(\text{\AA}^2)$
282.4		$0.0040 \pm 0.0002^b$		$0.0105 \pm 0.0008$	$0.0027 \pm 0.002$		
252.7		$0.018 \pm 0.003$		$0.017 \pm 0.002$	$0.011 \pm 0.002$		
228.7	$0.34 \pm 0.05$	$1.2 \pm 0.1$	$0.17 \pm 0.03$	$1.7 \pm 0.7$	$0.6 \pm 0.1$	$0.73 \pm 0.06$	$0.5 \pm 0.1$
217.8	$0.7 \pm 0.2$	$2.3 \pm 0.4$	$0.19 \pm 0.07$	$2.4 \pm 0.4$	$0.83 \pm 0.07$	$1.5 \pm 0.4$	$0.74 \pm 0.08$
208.9	$0.9 \pm 0.1$	$4.3 \pm 0.8$	$1.1 \pm 0.3$	$3.6 \pm 0.4$	$1.5 \pm 0.4$	$2.4 \pm 0.5$	$1.5 \pm 0.3$
204.3	$1.1 \pm 0.1$	$4.1 \pm 0.9$	$0.7 \pm 0.3$	$3.3 \pm 0.6$	$1.3 \pm 0.4$	$3.0 \pm 1.0$	$1.7 \pm 0.4$
192.2	$0.44 \pm 0.07$	$1.6 \pm 0.4$	$0.60 \pm 0.06$	$2.4 \pm 0.6$	$0.59 \pm 0.08$	$1.4 \pm 0.7$	$1.2 \pm 0.3$

<sup>a</sup> Absolute Raman scattering cross sections. These values were determined by comparison to the 802-cm<sup>-1</sup> mode of cyclohexane as described in the text. <sup>b</sup> Errors represent standard deviation from the mean.

**TABLE 3: Absolute Raman Cross Sections of Nitrosyl Chloride Dissolved in Acetonitrile**

excitation $\lambda$ (nm)	$\nu_1$ $\times 10^7(\text{\AA}^2)^a$	$\nu_2$ $\times 10^7(\text{\AA}^2)$	$\nu_3$ $\times 10^7(\text{\AA}^2)$	$2\nu_3$ $\times 10^7(\text{\AA}^2)$	$\nu_2 + \nu_3$ $\times 10^7(\text{\AA}^2)$
355		$0.00058 \pm 0.00009^b$	$0.0014 \pm 0.0001^b$	$0.000037 \pm 0.000005$	
282.4		$0.026 \pm 0.001$	$0.035 \pm 0.003$	$0.0080 \pm 0.0009$	$0.015 \pm 0.002$
252.7		$0.25 \pm 0.02$	$0.28 \pm 0.05$	$0.15 \pm 0.01$	$0.22 \pm 0.03$
228.7		$0.77 \pm 0.03$	$1.6 \pm 0.2$	$0.53 \pm 0.10$	$0.60 \pm 0.09$
217.8		$1.30 \pm 0.4$	$2.0 \pm 0.5$	$0.84 \pm 0.09$	$0.9 \pm 0.1$
208.9		$1.6 \pm 0.2$	$2.2 \pm 0.6$	$0.87 \pm 0.08$	$0.9 \pm 0.3$
204.3		$1.1 \pm 0.2$	$1.7 \pm 0.4$	$0.63 \pm 0.04$	
192.2		$0.35 \pm 0.03$	$0.7 \pm 0.3$	$0.10 \pm 0.02$	

<sup>a</sup> Absolute Raman scattering cross sections. These values were determined by comparison to the 918-cm<sup>-1</sup> mode of acetonitrile as described in the text. <sup>b</sup> Errors represent 1 standard deviation from the mean.

observation demonstrates that the curvature of the ground-state potential energy surface is solvent-dependent. Similar behavior was observed in our earlier study of ClNO in cyclohexane where the frequencies of the observed transitions were compared to those reported by Kinsey and co-workers for gaseous ClNO, and significant differences were evident.<sup>25,32</sup>

The excited-state potential energy surface parameters were determined by simultaneously modeling the absorption cross sections, absolute resonance Raman cross sections, and depolarization ratios. In the modeling, the broadening was assumed to be all homogeneous. Inhomogeneous broadening was not included because inclusion in the two-state model requires the assumption that the inhomogeneous broadening between states be correlated. Given the severity of such an assumption, we chose not to incorporate inhomogeneous broadening in the spectroscopic modeling. The experimental (solid lines) and calculated (dashed lines) absorption cross sections for ClNO dissolved in cyclohexane and acetonitrile are presented in Figure 4A and B, respectively. The corresponding fit parameters are presented in Tables 4 and 5, respectively. An inspection of Figure 4A and B demonstrates that the reproduction of the experimental absorption spectrum is reasonable but that the red-edge intensity is underestimated by the model. Figures 5 and 6 present the experimental and predicted Raman excitation profiles for ClNO dissolved in cyclohexane and acetonitrile, respectively. The figures provide a comparison of the Raman cross sections for the N–Cl stretch fundamental ( $\nu_2$ ), the bend fundamental ( $\nu_3$ ), the bend overtone ( $2\nu_3$ ), and the combination band involving these coordinates ( $\nu_2 + \nu_3$ ). The N=O stretch fundamental ( $\nu_1$ ) is observed in cyclohexane, and the results for this transition are also presented in Figure 5. In summary, the model accurately reproduces the observed Raman cross sections. An inspection of the excited-state parameters presented in Tables 4 and 5 demonstrates that relatively large displacements are required to reproduce the observed intensities for the bend and that a large excited-state slope along the dissociative N–Cl stretch is also required, consistent with these coordinates dominating the excited-state structural evolution that occurs upon photoexcitation. Correspondingly, the modest intensity of

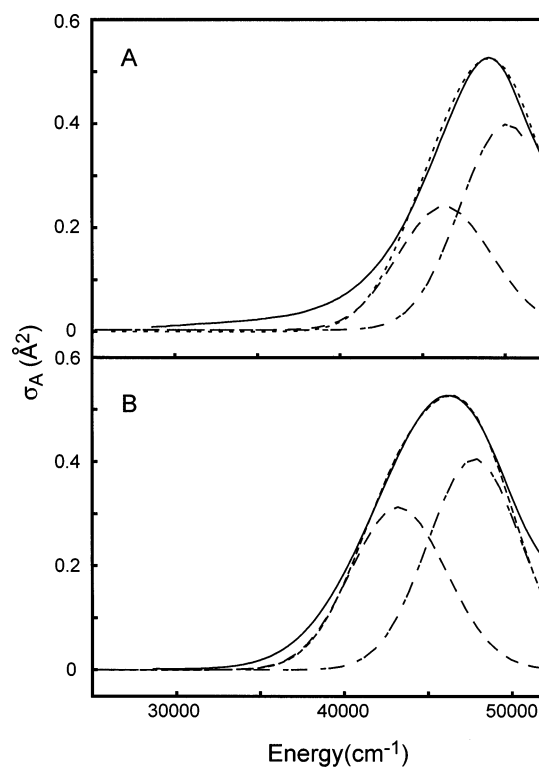


**Figure 4.** Experimental electronic absorption spectra (—), and calculated spectra (---) for ClNO in cyclohexane (A) and acetonitrile (B). Individual absorption transitions are also indicated by the long dashed and dot-dashed lines. The parameters employed in the calculations are presented in Tables 4 and 5.

the N=O stretch in cyclohexane, and no assignable intensity in acetonitrile, is indicative of limited excited-state evolution along this coordinate.

In the dissociative two-excited-states model, the homogeneous line widths were found to increase substantially between cyclohexane ( $\Gamma_1 = 200$  cm<sup>-1</sup>,  $\Gamma_2 = 350$  cm<sup>-1</sup>) and acetonitrile ( $\Gamma_1 = 1200$  cm<sup>-1</sup>,  $\Gamma_2 = 1300$  cm<sup>-1</sup>). This increase is supported spectroscopically by the depression of the resonance Raman

**TABLE 4: Excited-State Parameters for Nitrosyl Chloride in Cyclohexane<sup>a</sup>**

transition <sup>b</sup>	$\omega_g$ (cm <sup>-1</sup> ) <sup>c</sup>	$\omega_e$ (cm <sup>-1</sup> )	$\Delta^d$	$\beta^e$ (cm <sup>-1</sup> )	$\sigma_R$ expt <sup>f</sup> ( $\times 10^7 \text{ \AA}^2$ )	$\sigma_R$ calcd ( $\times 10^7 \text{ \AA}^2$ )
State 1						
$\nu_1$	1800	1800	0.85		$1.1 \pm 0.1$	1.0
$\nu_2$	585	585		2750	$4.1 \pm 0.9$	3.6
$\nu_3$	325	325	7.70		$3.3 \pm 0.6$	3.0
$3\nu_2$					$0.7 \pm 0.3$	0.4
$2\nu_3$					$1.3 \pm 0.4$	0.9
$\nu_2 + \nu_3$					$3.0 \pm 1.0$	2.0
$\nu_2 + 2\nu_3$					$1.7 \pm 0.4$	1.1
State 2						
$\nu_1$	1800	1800	0.78		$1.1 \pm 0.1$	1.0
$\nu_2$	585	585		2750	$4.1 \pm 0.9$	3.6
$\nu_3$	325	325	7.65		$3.3 \pm 0.6$	3.0
$3\nu_2$					$0.7 \pm 0.3$	0.4
$2\nu_3$					$1.3 \pm 0.4$	0.9
$\nu_2 + \nu_3$					$3.0 \pm 1.0$	2.0
$\nu_2 + 2\nu_3$					$1.7 \pm 0.4$	1.1

<sup>a</sup> Calculation performed with a Gaussian homogeneous line width. Best fit to the experimental cross sections yielded for state 1  $\Gamma = 200 \pm 10 \text{ cm}^{-1}$ ,  $M_1 = 0.93 \text{ \AA}$ ,  $E_{00} = 39\,700 \text{ cm}^{-1}$ ,  $n = 1.42$  and for state 2  $\Gamma = 350 \pm 10 \text{ cm}^{-1}$ ,  $M_2 = 0.75 \text{ \AA}$ ,  $E_{00} = 36\,050 \text{ cm}^{-1}$ , and  $n = 1.42$ . <sup>b</sup> Raman transition that is being modeled by this calculation. The symbols  $\nu_1$ ,  $\nu_2$ , and  $\nu_3$  correspond to the N–O stretch and the N–Cl stretch and bend, respectively. The first three terms refer to the fundamental transitions; the second three, to overtones; and the last two, to combination bands. <sup>c</sup>  $\omega_g$  is the ground-state harmonic frequency, and  $\omega_e$  is the excited-state harmonic frequency. <sup>d</sup>  $\Delta$  refers to the dimensionless displacement of the excited-state potential energy surface minimum relative to the ground state. <sup>e</sup>  $\beta$  refers to the slope of the dissociative excited-state potential. <sup>f</sup> Experimental Raman cross sections found for excitation at 204.3 nm.

**TABLE 5: Excited-State Parameters for Nitrosyl Chloride in Acetonitrile<sup>a</sup>**

transition <sup>b</sup>	$\omega_g$ (cm <sup>-1</sup> ) <sup>c</sup>	$\omega_e$ (cm <sup>-1</sup> )	$\Delta^d$	$\beta^e$ (cm <sup>-1</sup> )	$\sigma_R$ expt <sup>f</sup> ( $\times 10^7 \text{ \AA}^2$ )	$\sigma_R$ calcd ( $\times 10^7 \text{ \AA}^2$ )
State 1						
$\nu_1$	1780	1780	0.00			
$\nu_2$	545	545		1850	$1.1 \pm 0.2$	1.1
$\nu_3$	310	310	7.70		$1.7 \pm 0.4$	1.9
$2\nu_3$					$0.63 \pm 0.04$	0.68
$\nu_2 + \nu_3$						
State 2						
$\nu_1$	1780	1780	0.00			
$\nu_2$	545	545		1850	$1.1 \pm 0.2$	1.1
$\nu_3$	310	310	7.65		$1.7 \pm 0.4$	1.9
$2\nu_3$					$0.63 \pm 0.04$	0.68
$\nu_2 + \nu_3$						

<sup>a</sup> Calculation performed with a Gaussian homogeneous line width. Best fit to the experimental cross sections yielded for state 1  $\Gamma = 1200 \pm 10 \text{ cm}^{-1}$ ,  $M_1 = 0.905 \text{ \AA}$ ,  $E_{00} = 38\,450 \text{ cm}^{-1}$ , and  $n = 1.344$  and for state 2  $\Gamma = 1300 \pm 10 \text{ cm}^{-1}$ ,  $M_2 = 0.85 \text{ \AA}$ ,  $E_{00} = 34\,050 \text{ cm}^{-1}$ , and  $n = 1.344$ . <sup>b</sup> Raman transition that is being modeled by this calculation. The symbols  $\nu_1$ ,  $\nu_2$ , and  $\nu_3$  correspond to the N–O stretch and the N–Cl stretch and bend, respectively. The first three terms refer to the fundamental transitions; the second three, to overtones; and the last two, to combination bands. <sup>c</sup>  $\omega_g$  is the ground-state harmonic frequency, and  $\omega_e$  is the excited-state harmonic frequency. <sup>d</sup>  $\Delta$  refers to the dimensionless displacement of the excited-state potential energy surface minimum relative to the ground state. <sup>e</sup>  $\beta$  refers to the slope of the dissociative excited-state potential. <sup>f</sup> Experimental Raman cross sections found for excitation at 204.3 nm.

cross sections for ClNO in acetonitrile relative to those for ClNO in cyclohexane. The values for  $\Gamma$  in both solvents suggests rapid excited-state decay, a conclusion that is supported by the lack of detectable fluorescence in either solvent. The  $E_{00}$  separation of the two states is larger in acetonitrile ( $4450 \text{ cm}^{-1}$ ) compared

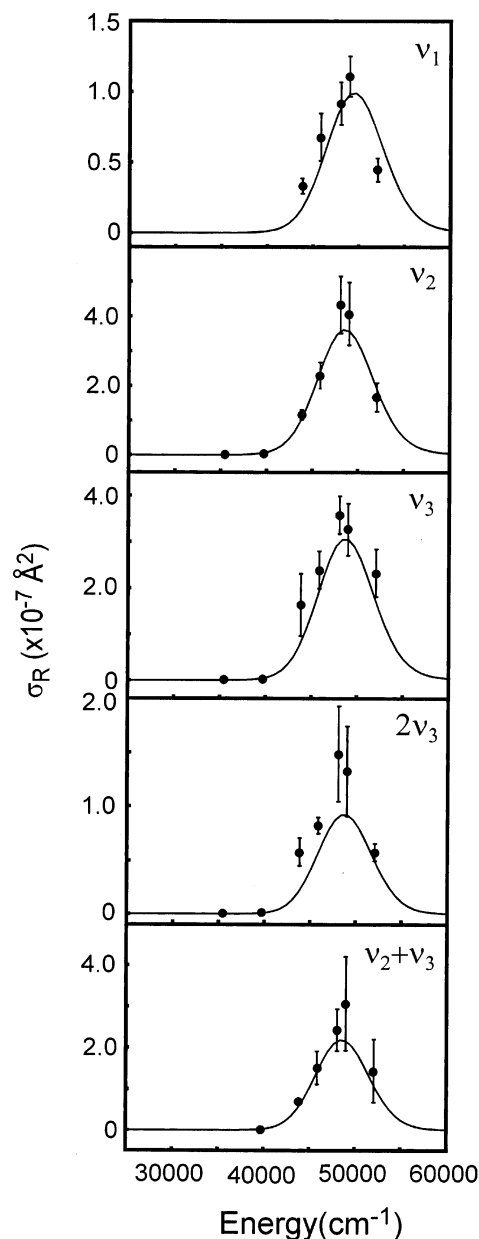


**Figure 5.** Raman excitation profiles for the NO stretch fundamental ( $\nu_1$ ), the N–Cl stretch fundamental ( $\nu_2$ ), the bend fundamental ( $\nu_3$ ), the bend overtone ( $2\nu_3$ ), and the combination band ( $\nu_2 + \nu_3$ ) for ClNO in cyclohexane. Points represent the experimental data, and the error bars represent 1 standard deviation from the mean. The parameters for a calculated fit (—) are presented in Table 4.

to that in cyclohexane ( $3650 \text{ cm}^{-1}$ ), consistent with the excited-state energetics being solvent-dependent. Finally, the slopes along the dissociative potential of the N–Cl stretch were observed to decrease from cyclohexane ( $\beta = 2750 \text{ cm}^{-1}$ ) to acetonitrile ( $\beta = 1850 \text{ cm}^{-1}$ ). This evolution suggests that solvent–solute interactions are impacting the dissociation dynamics along the N–Cl stretch coordinate, an observation that will be discussed in detail below.

The measured resonance Raman depolarization ratios for the fundamental transitions of the N–Cl stretch ( $\nu_2$ ) and bend ( $\nu_3$ ) are reported in Table 6 and are presented in Figure 7A and B for ClNO dissolved in cyclohexane and acetonitrile, respectively. The depolarization ratios all deviate significantly from  $1/3$ , consistent with more than a single excited state participating in the scattering process. Although the experimental depolarization ratios deviate from the single-state value of  $1/3$ , they are also

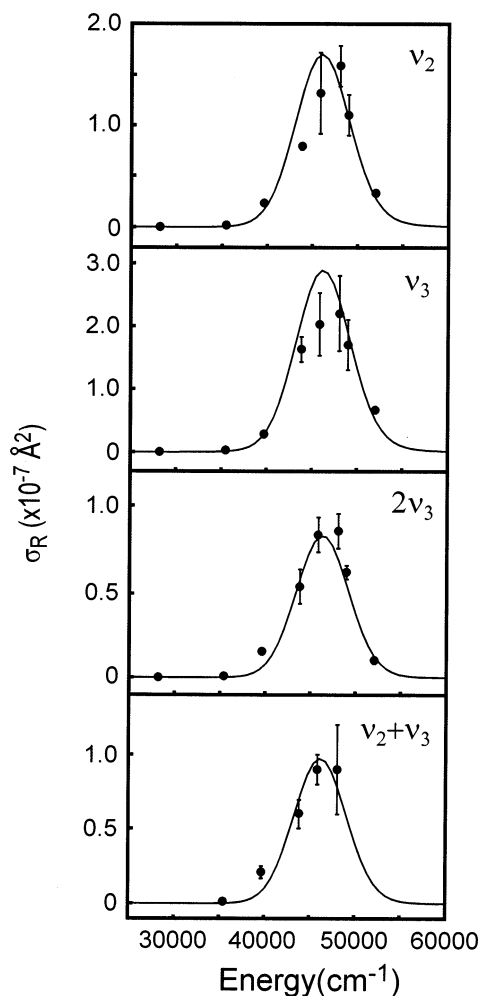


**Figure 6.** Raman excitation profiles for the N–Cl stretch fundamental ( $\nu_2$ ), the bend fundamental ( $\nu_3$ ), the bend overtone ( $2\nu_3$ ), and the combination band ( $\nu_2 + \nu_3$ ) for ClNO in acetonitrile. The points represent the experimental data, and the error bars represent 1 standard deviation from the mean. The parameters for a calculated fit (—) are presented in Table 5.

not consistent with two totally degenerate transitions for which  $\rho = 1/8$ . Therefore, the wavelength dependence of the depolarization ratios suggests that the two states contributing to the scattering are not totally degenerate. For the dissociative two-excited-states model, the depolarization dispersion curves are best reproduced using the parameters in Tables 4 and 5, and the corresponding fits to the data are shown in Figure 7. An inspection of Figure 7 demonstrates that the excited-state model employed does a reasonable job of reproducing the wavelength evolution of the depolarization ratios. Significant deviations are observed between the model and experimental results for the N–Cl stretch fundamental ( $\nu_2$ ) in acetonitrile at low-energy excitation wavelengths; however, the experimental results are compromised by the weakness of the scattering intensity at these wavelengths.

## Discussion

**Nature of the A Band.** The results presented here establish that the A band is composed of at least two overlapping electronic transitions. The experimental resonance Raman depolarization ratios presented in Table 6 for both solvents deviate significantly from the single-state value of  $1/3$ , demonstrating that more than a single excited state must be contributing to the scattering. The ability of a two-state model to reproduce

**TABLE 6: Depolarization Ratios for Nitrosyl Chloride in Cyclohexane and Acetonitrile**

excitation wavelength (nm)	$\rho(\nu_3)^a$	$\rho(\nu_2)$
Cyclohexane		
282.4	$0.18 \pm 0.02^b$	$0.14 \pm 0.03$
(calcd)	(0.13)	(0.13)
252.7	$0.20 \pm 0.03$	$0.15 \pm 0.04$
(calcd)	(0.17)	(0.17)
228.7	$0.25 \pm 0.05$	$0.21 \pm 0.04$
(calcd)	(0.27)	(0.26)
217.8	$0.28 \pm 0.03$	$0.23 \pm 0.04$
(calcd)	(0.31)	(0.31)
Acetonitrile		
354.7	$0.18 \pm 0.02^b$	$0.27 \pm 0.02$
(calcd)	(0.14)	(0.14)
282.4	$0.23 \pm 0.05$	$0.32 \pm 0.03$
(calcd)	(0.19)	(0.19)
252.7	$0.29 \pm 0.01$	$0.33 \pm 0.01$
(calcd)	(0.28)	(0.28)
228.7	$0.35 \pm 0.04$	$0.35 \pm 0.03$
(calcd)	(0.39)	(0.38)
217.8	$0.36 \pm 0.05$	$0.36 \pm 0.04$
(calcd)	(0.40)	(0.39)

<sup>a</sup> Raman depolarization ratios are defined as the scattered intensity with polarization perpendicular to that of the incident radiation divided by the scattered intensity with polarization parallel to that of the incident radiation. <sup>b</sup> Errors represent 1 standard deviation from the mean of four to seven measurements depending on the excitation wavelength.

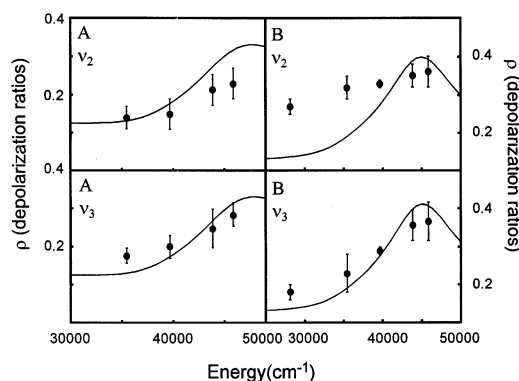


**Figure 7.** Experimental depolarization ratios (●) for ClNO in cyclohexane (A) and ClNO in acetonitrile (B) corresponding to the N–Cl stretch fundamental ( $\nu_2$ ) and the bend fundamental ( $\nu_3$ ). The best fits to the data (—) were calculated using the parameters reported in Tables 6 and 5, respectively.

the depolarization dispersion curves (Figure 7) further confirms the multitransition composition of the A band. The conclusion that the A band is composed of more than a single electronic transition is supported by numerous gas-phase experiments that suggest that more than one electronic surface is accessed following A-band photoexcitation. For example, a bimodal photoproduct translational-energy distribution was observed in a photofragment translational-spectroscopy experiment employing excitation resonance with the A band, suggesting that there are two separate photodissociation pathways arising from two excited states.<sup>15</sup> In addition, photofragment anisotropy studies have been interpreted in terms of at least two states comprising the A band.<sup>12,14</sup> Ab initio studies by Bai et al. predict that more than a single electronic transition resides in the A band and suggest that as many as three electronic transitions exist in this wavelength region, including a weak single–triplet transition.<sup>8</sup> This suggestion is interesting in light of the difficulty in modeling the red edge of the absorption spectrum (Figure 4). Specifically, the absorption cross sections at lower frequency

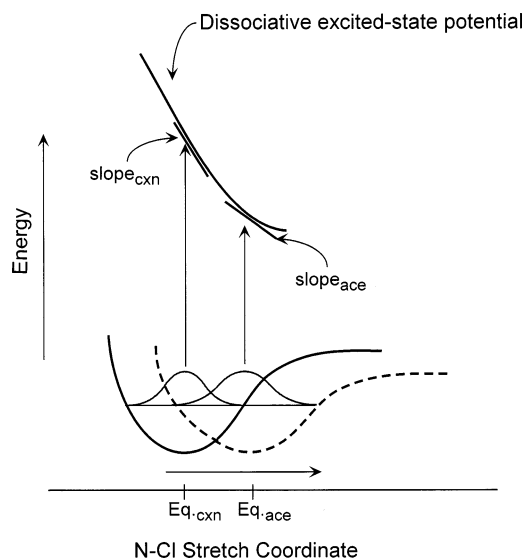


**Figure 8.** N–Cl stretch undergoing a change in displacement due to the solvent environment. Shown is the dissociative potential for the weakly bound N–Cl stretch and how solvent affects the excited-state slope for CINO in cyclohexane (—) and acetonitrile (---).

are not accurately reproduced by the two-state model employed here, suggesting that a third state might also be present. The contribution of triplet states to the absorption and resonance Raman cross section is expected to be extremely modest given the limited transition moment of single–triplet transitions. Therefore, the reasons for the discrepancy between the experimental and model cross sections at lower frequency remain to be explored.

**Excited-State Evolution.** The resonance Raman data reported here provides a mode-specific description of the excited-state structural evolution that occurs following CINO photoexcitation resonant with the A band in solution. First, the modeling demonstrates that the excited-state structural evolution is dominated by motion along the N–Cl stretch and bend coordinates. Because the N–Cl bond dissociates upon photoexcitation, structural excited-state evolution along this coordinate is perhaps expected. However, the results presented here point to the surprising result that the excited-state structural evolution is solvent-dependent, with two features of the excited-state potential energy surfaces changing with solvent: the slope ( $\beta$ ) of the linearly dissociative potential and the  $E_{00}$  energies. The increase in  $E_{00}$  separation between the two excited states in acetonitrile relative to that in cyclohexane demonstrates that these two states are solvated to differing extents as the polarity of the solvent is increased, thereby suggesting that the charge distribution of these states must be different. High-level *ab initio* calculations would provide substantial insight into the origin of this differential solvation.

The modeling also demonstrates that the slope of the dissociative excited-state potential along the N–Cl stretch is solvent-dependent. Specifically, the slope along this coordinate decreases from  $\beta = 2750$  to  $1850 \text{ cm}^{-1}$  for both states between cyclohexane and acetonitrile. The magnitude of the homogeneous line width employed dictates that the resonance Raman intensities are sensitive to the slope of the excited state in the Franck–Condon region exclusively. Therefore, the question is why would the slope of the excited state in the Franck–Condon region change as a function of solvent? We propose that the change in the slope reflects the solvent dependence of the ground-state equilibrium N–Cl bond distance. This idea is illustrated in Figure 8. In CINO, the N–Cl bond is extremely

weak as demonstrated by a ground-state N=O bond length ( $1.14 \text{ \AA}$ ) that is nearly identical to the bond length for the free NO ( $1.151 \text{ \AA}$ ).<sup>47</sup> This similarity in N=O bond lengths dictates that an extremely modest excited-state displacement exists along the N=O stretch coordinate, consistent with the modeling results. As the polarity of the solvent is increased, the N–Cl bond length is weakened corresponding to a shift of the ground-state potential energy surface minimum along the N–Cl coordinate. Shifting of the ground-state minimum to larger N–Cl distances is expected to result in a decrease of the excited-state slope in the Franck–Condon region, as observed in the modeling. One important prediction of this model is that the absorption spectrum should shift to lower frequencies in polar solvents. This is exactly the behavior observed in Figure 1 as one goes from the gas-phase spectrum of CINO to that of CINO dissolved in cyclohexane and acetonitrile. A second prediction of this model is that the frequency of the N–Cl stretch should decrease in acetonitrile relative to that in cyclohexane, an expectation that is supported experimentally as illustrated in Figure 2. This is also further born out by a comparison of the transition frequencies in the gas-phase study by Kinsey et al. to those presented in our earlier study of CINO in cyclohexane where a noticeable change in frequencies is observed.<sup>25,32</sup>

**Homogeneous Broadening.** The results presented here demonstrate that the homogeneous line width increases significantly as the solvent is changed from cyclohexane to acetonitrile. Absolute resonance Raman cross sections are dependent upon the magnitude of the homogeneous broadening, and a comparison of the absolute scattering cross sections in these solvents demonstrates that the cross sections in acetonitrile are substantially reduced relative to those in cyclohexane (Tables 2 and 3). The increase in homogeneous broadening in acetonitrile compared to that in cyclohexane is also supported spectroscopically by the relative dearth of overtone and combination band intensity in the CINO resonance Raman spectrum obtained in acetonitrile (Figure 3).

The question exists as to why the homogeneous line width should be solvent-dependent for excited states that are dissociative in character. The homogeneous line width ( $\Gamma$ ) is composed of two parts: the lifetime of the excited state and solvent-induced pure dephasing. In the modeling, the separation of  $E_{00}$  energies was observed to increase between acetonitrile and cyclohexane. This change in  $E_{00}$  energies could alter state coupling and subsequent nonadiabatic relaxation dynamics, thereby affecting  $\Gamma$ . To test this hypothesis, time-resolved experiments are currently underway to study the excited-state lifetime and photoproduct formation kinetics of CINO to ascertain the role of solvent-induced dephasing of CINO in solution.

## Conclusions

We have performed an absolute resonance Raman intensity analysis study of CINO dissolved in cyclohexane and acetonitrile. The resonance Raman spectra demonstrate that significant excited-state structural evolution occurs along the bend and the dissociative N–Cl stretch coordinate upon A-band photoexcitation. The excited-state slope along the N–Cl stretch coordinate is solvent-dependent and related to the structural evolution of the ground-state equilibrium geometry with solvent. Modest scattering intensity corresponding to the N=O stretch coordinate was observed in cyclohexane but not in acetonitrile. This limited intensity suggests that the excited-state structural evolution that occurs along this coordinate following photoexcitation is modest. Resonance Raman depolarization ratios are found to deviate

significantly from  $1/3$ , consistent with the A band being composed of at least two separate electronic transitions. Therefore, modeling of the absorption, absolute resonance Raman cross sections, and depolarization ratios was performed with two excited states contributing to the spectroscopic observables. This model is capable of simultaneously reproducing the experimental observables consistent with the A-band intensity originating from transitions to at least two excited states.

**Acknowledgment.** The National Science Foundation is acknowledged for its support of this work (CHE-0091320). Acknowledgment is also made to the donors of the Petroleum Research Fund, administered by the American Chemical Society. P.J.R. is the recipient of an Alfred P. Sloan Fellowship and is a Cottrell Scholar of the Research Corporation.

## References and Notes

- Colburn, C. B. *Developments in Inorganic Nitrogen Chemistry*; Elsevier: New York, 1973.
- Finlayson-Pitts, B. J.; Pitts, J. N. *Chemistry in the Upper and Lower Atmosphere*; Academic Press: New York, 2000.
- Luick, T. J.; Heckert, R. W.; Schultz, K.; Disselkamp, R. S. *J. Atmos. Chem.* **1999**, *32*, 315.
- Engelman, R.; Rouse, P. E. *J. Mol. Spectrosc.* **1971**, *37*, 240.
- Moser, M. D.; Weitz, E.; Schatz, G. C. *J. Chem. Phys.* **1983**, *78*, 757.
- Bechara, J.; Morrow, T.; McGrath, W. D. *Chem. Phys. Lett.* **1985**, *122*, 605.
- Ticktin, A.; Bruno, A. E.; Bruhlmann, U.; Huber, J. R. *Chem. Phys.* **1988**, *125*, 403.
- Bai, Y. Y.; Ogai, A.; Iwata, L.; Segal, G. A.; Reisler, H. *J. Chem. Phys.* **1989**, *90*, 3903.
- Qian, C. X. W.; Ogai, A.; Iwata, L.; Reisler, H. *J. Chem. Phys.* **1990**, *92*, 4296.
- Ogai, A.; Qian, C. X. W.; Reisler, H. *J. Chem. Phys.* **1990**, *93*, 1107.
- Cao, J.; Wang, Y.; Qian, C. X. W. *J. Chem. Phys.* **1995**, *103*, 9653.
- Haas, B. M.; Felder, P.; Huber, J. R. *Chem. Phys. Lett.* **1991**, *180*, 293.
- Gillan, I. T. F.; Denvir, D. J.; Cormican, H. F. J.; Duncan, I.; Morrow, T. *Chem. Phys.* **1992**, *167*, 193.
- Felder, P.; Morley, G. P. *Chem. Phys.* **1994**, *185*, 145.
- Skorokhodov, V.; Sato, Y.; Suto, K.; Matsumi, Y.; Kawasaki, M. *J. Phys. Chem.* **1996**, *100*, 12321.
- Goodeve, C. F.; Katz, S. *Proc. R. Soc. London, Ser. A* **1939**, *172*, 432.
- Ballash, N. M.; Armstrong, D. A. *Spectrochim. Acta, Part A* **1974**, *30*, 941.
- Reisler, H.; Qian, C. In *Advances in Molecular Vibrations and Collision Dynamics*; Bowman, J. M., Ed.; JAI Press: Greenwich, CT, 1991; Vol. 1B.
- Qian, C. X. W.; Ogai, A.; Brandon, J.; Bai, Y. Y.; Reisler, H. *J. Phys. Chem.* **1991**, *95*, 6763.
- Loock, H. P.; Cao, J.; Qian, C. X. W. *Chem. Phys. Lett.* **1993**, *206*, 422.
- Demyanenko, A. V.; Dribinski, V.; Reisler, H.; Meyer, H.; Qian, C. X. W. *J. Chem. Phys.* **1999**, *111*, 7383.
- Kable, S. H.; Loison, J.-C.; Neyer, D. W.; Houston, P. L.; Burak, I.; Dixon, R. N. *J. Phys. Chem.* **1991**, *95*, 8013.
- Solgadi, D.; Lahmani, F.; Lardeux, C. *Chem. Phys.* **1983**, *79*, 225.
- Lacombe, S.; Loudet, M.; Dargelos, A.; Camou, J. M. *Chem. Phys.* **2000**, *258*, 1.
- Mackey, J. L.; Johnson, B. R.; Kittrell, C.; Lee, L. D.; Kinsey, J. L. *J. Chem. Phys.* **2001**, *114*, 6631.
- Hallou, A.; Schriver-Mazzuoli, L.; Schriver, A.; Chaquin, P. *Chem. Phys.* **1998**, *237*, 251.
- Maier, G.; Reisenauer, H. P.; De Marco, M. *Chem.—Eur. J.* **2000**, *6*, 800.
- Ning, C.; Pfab, J. *Chem. Phys. Lett.* **1993**, *216*, 87.
- McDonald, J. K.; Merritt, J. A.; Kalasinsky, V. F.; Huesel, H. L.; Durig, J. R. *J. Mol. Spectrosc.* **1986**, *117*, 69.
- Bell, A. J.; Pardon, P. R.; Frey, J. G. *Mol. Phys.* **1989**, *67*, 465.
- Bell, A. J.; Frey, J. G. *Mol. Phys.* **1990**, *69*, 943.
- Barham, B. P.; Reid, P. J. *Chem. Phys. Lett.* **2002**, *361*, 49.
- Pass, G.; Sutcliffe, H. *Practical Inorganic Chemistry: Preparation, Reactions and Instrumental Methods*; Chapman and Hall: London, 1968.
- Mortensen, O. S.; Hassing, S. In *Advances in Infrared and Raman Spectroscopy*; Clark, R. J. H., Hester, R. E., Eds.; Heyden: London, 1980; Vol. 6.
- Dawson, P. *Spectrochim. Acta, Part A* **1972**, *28*, 715.
- Dudik, J. M.; Johnson, C. R.; Asher, S. A. *J. Chem. Phys.* **1985**, *82*, 1732.
- Li, B.; Myers, A. B. *J. Phys. Chem.* **1990**, *94*, 4051.
- Hess, R. H., H.; Schrotter, H. W.; Brandmuller, J. *Z. Angew. Phys.* **1969**, *27*, 233.
- Myers, A. B. *J. Raman Spectrosc.* **1997**, *28*, 389.
- Myers, A. B.; Mathies, R. A. In *Biological Applications of Raman Spectroscopy*; Spiro, T. G., Ed.; Wiley & Sons: New York, 1987; Vol. 2.
- Lee, S.-Y.; Heller, E. J. *J. Chem. Phys.* **1979**, *71*, 4777.
- Myers, T. L.; Kitchen, D. C.; Hu, B.; Butler, L. J. *J. Chem. Phys.* **1996**, *104*, 5446.
- Mukamel, S. *J. Chem. Phys.* **1985**, *82*, 5398.
- Loppnow, G. R.; Mathies, R. A. *Biophys. J.* **1988**, *54*, 35.
- Zgierski, M. Z.; Pawlikowski, M.; Hudson, B. S. *J. Chem. Phys.* **1995**, *103*, 1361.
- Okabe, H. In *Photochemistry of Small Molecules*; Wiley-Interscience; New York, 1978; p 170.
- Miessler, G. L.; Tarr, D. A. *Inorganic Chemistry*; Prentice Hall: Englewood Cliffs, NJ, 1991; p 250.